Applied Catalysis A: General 449 (2012) 81–87

Contents lists available at SciVerse ScienceDirect

Applied Catalysis A: General

journal homepage: www.elsevier.com/locate/apcata

Selective gas phase hydrogenation of maleic anhydride over Ni-supported catalysts: Effect of support on the catalytic performance

Silvina A. Regenhardt, Camilo I. Meyer, Teresita F. Garetto, Alberto J. Marchi*

Catalysis Science and Engineering Research Group (GICIC), Instituto de Investigaciones en Catálisis y Petroquímica (INCAPE), FIQ-UNL-CONICET, Santiago del Estero 2654 (3000) Santa Fe, Argentina

ARTICLE INFO

Article history:
Received 9 August 2012
Received in revised form
12 September 2012
Accepted 21 September 2012
Available online 8 October 2012

Keywords:
Hydrogenation
Hydrogenolysis
Ni-based catalysts
γ-Butyrolactone

ABSTRACT

The gas phase hydrogenation of maleic anhydride to obtain γ-butyrolactone was studied using Ni supported on SiO_2, SiO_2–Al_2O_3 and zeolite H-BEA as catalysts. The samples were prepared by incipient wetness impregnation and characterized by N_2 adsorption at −196 °C (*Sg*), X-ray diffraction (XRD), temperature programmed reduction (TPR), temperature programmed desorption of NH_3 (TPD-NH_3) and chemisorption of H_2. The reaction was carried out at 170 °C and 220 °C in a fixed bed reactor operating at atmospheric pressure. From the characterization results, it was determined that the degree of Ni^{2+}–support interaction varies according to the following pattern: Ni/HBEA > Ni/SiO_2–Al_2O_3 > Ni/SiO_2. All catalysts were very active in the hydrogenation of maleic anhydride to succinic anhydride. However, hydrogenolytic activity and stability of nickel-based catalyst varies with the degree of interaction Ni^{2+}–support. Ni/H-BEA, in which Ni^{2+}–support interaction is the highest, was active in the hydrogenolysis of succinic anhydride to γ-butyrolactone but it was not stable. By contrast, Ni/SiO_2–Al_2O_3 and Ni/SiO_2, with medium or low degree of Ni^{2+}–support interaction, were more stable than Ni/H-BEA. In addition, Ni/SiO_2–Al_2O_3, with a medium degree of Ni^{2+}–support interaction, was the most stable and selective to γ-butyrolactone, especially when the reaction was carried out at 220 °C.

1. Introduction

The global reaction network for maleic anhydride (MA) hydrogenation over Ni-based catalysts is shown in Fig. 1. In this process, both hydrogenation and hydrogenolysis reactions are involved. Some of the possible reaction products, as succinic anhydride (SA), γ-gammabutyrolactone (GBL), tetrahydrofurane (THF), and 1,4-butanediol (BDO), are important starting materials in chemical industry. In particular, SA, the first product in the reaction sequence, is widely used in the manufacture of polymeric materials, pharmaceuticals, agrochemicals, dyes, photographic chemicals, surface active agents, lubricant additives, organic flame retardant materials, esters, flavors and fragrances. GBL is mainly used as solvent in replacement of chlorinated solvents and synthesis intermediate for the production of agrochemicals, pharmaceuticals and polymers [1,2].

In the open literature, several papers reported different type of catalysts and a variety of operating conditions in order to carry out the MA hydrogenation [1–10]. The reaction was studied using several types of noble metal-based catalysts, such as Pd, Pt and Au, both in liquid and gas phase [3,7–9]. Generally, the experiments were carried out in the temperature and pressure ranges of 190–240 °C and 1–5 MPa, respectively. Copper-based catalysts were also used to study the gas-phase hydrogenation of MA between 210 and 280 °C [4,10]. In general, the catalysts composition of these copper-based catalysts is rather complex since they also contain Al, Zn, Cr and Ce. In addition, the use of Cr-based catalysts is undesirable because hexavalent Cr ions are highly toxic. In all of the cases, the main products were SA, GBL, THF and BDO and the product distribution was strongly depending on the reaction conditions and the type of catalyst. Other by-products may also be obtained during MA hydrogenation, such as propionic acid (PA), methane and CO [5,6]. In some cases, partial catalyst deactivation has been reported for copper-based catalysts [10–12].

Despite the fact that there are many works in which an exhaustive study of the behavior of Ni, supported on mesoporous and microporous solids, in different hydrogenation–hydrogenolysis reactions was made [13,14], to our knowledge, there is not research work dealing with the study of support influence on the performance of Ni-based catalysts in the gas phase MA hydrogenation.

In a previous work we found evidence that Ni-based catalysts are active for MA hydrogenation and SA hydrogenolysis in gas phase [15]. In this work, we analyze the catalytic performance of Ni supported over different insulating oxides on the selective MA hydrogenation to GBL in gas phase at atmospheric pressure. The

* Corresponding author at: INCAPE (U.N.L. – CONICET), Santiago del Estero 2654, (S3000AOJ) Santa Fe, Argentina. Tel.: +54 342 457 1164/2747; fax: +54 342 453 1168.
E-mail address: amarchi@fiq.unl.edu.ar (A.J. Marchi).

0926-860X/$ – see front matter © 2012 Elsevier B.V. All rights reserved.
http://dx.doi.org/10.1016/j.apcata.2012.09.023

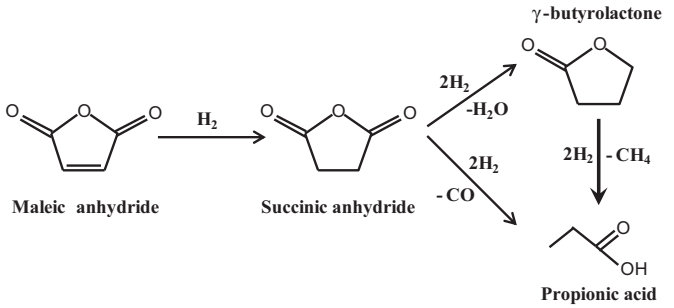

Fig. 1. Global reaction network for MA hydrogenation.

objective is to determine the influence of the support on the catalytic activity of Ni in order to improve the selectivity to GBL.

2. Experimental

2.1. Catalyst preparation and characterization

Different insulating oxides with distinct pore size and structure were used as supports: SiO_2 (Grace Davison Grade 62), SiO_2–Al_2O_3 (Sigma–Aldrich) and H-BEA (Chemie Uetikon). The catalysts were prepared by incipient wetness impregnation method using the corresponding volumes of $Ni(NO_3)_2$ solutions in order to obtain a theoretical metal loading of 10%. The hydrated precursors, obtained after impregnation, were dried at 120 °C overnight and then calcinated in air flow at 500 °C for 2 h. The experimental nickel loading was determined by using ICP (Inductively Coupled Plasma) analysis.

The specific surface area and pore distribution of the oxide precursor, obtained after impregnation and calcination, were determined by N_2 physisorption at −196 °C using a Quantachrome Autosorb-1 sorptometer. Samples were previously degassed at 250 °C under vacuum.

The reducibility of nickel oxide species was determined by TPR (temperature programmed reduction) using a Micromeritics AutoChem 2920 system equipped with a thermal conductivity detector. The TPR profiles were obtained passing a H_2(5%)/Ar gas stream (60 cm^3/min STP), while the temperature was increased from 25 to 800 °C at 10 °C/min.

XRD data was recorded at room temperature by employing a Shimadzu D-1 diffractometer and using Cu-Kα radiation (λ = 1.5418 Å) and a Ni filter. Analysis was carried out using a continuous scan mode at 2 °C/min in the range 2θ = 10–80°. Crystallite mean size was calculated from the half-with of the NiO (1 1 1) diffraction line by applying Debye–Scherrer equation.

Chemisorption of hydrogen was measured by carrying out volumetric adsorption experiments at room temperature in a conventional vacuum unit equipped with MKS Baratron pressure gauge. Catalysts were reduced in H_2 at 500 °C for 2 h and then outgassed 2 h at 500 °C prior to performing gas chemisorption experiments. Hydrogen uptake was determined using double isotherm method. After cooling to room temperature a first isotherm (primary isotherm) was drawn for measuring the total H_2 uptake. Then, after 1 h of evacuation at room temperature, a second isotherm (secondary isotherm) was performed to determine the amount of weakly adsorbed H_2. The amount of irreversibly held H_2 $(HC)_i$, was calculated as the difference between total and weakly adsorbed H_2. The pressure range of isotherms was 0–6.6 kPa.

Acid site densities were determined by NH_3 TPD (temperature programmed desorption). Samples (200 mg) were treated in He flow (~60 cm^3 min^{-1}) at 500 °C for 1.5 h and exposed to a NH_3(1%)/He stream at 100 °C until surface saturation. Weakly adsorbed NH_3 was removed by flowing He at 60 cm^3 min^{-1} for 0.5 h. Temperature was then increased to 600 °C at 10 °C min^{-1}, and the NH_3 concentration in the effluent was measured by mass spectroscopy (MS) using a Baltzers Omnistar unit. The monitored signals during this analysis were m/e = 2, 16, 17, 18 and 28.

2.2. Catalytic activity

The hydrogenation of MA in gas phase was performed at atmospheric pressure in a fixed-bed tubular reactor (SS 1.5 cm i.d.) operated by down flow mode. Samples were pressed to obtain tablets that were then crushed and screening. The fraction in the range of 0.35–0.42 mm was loaded to the reactor after dilution with quartz using a quartz/catalyst ratio of 1. Catalyst loading (W) of 0.050 g, contact time (W/F^0_{MA}) of 12 g cat. h mol^{-1} MA and gas flow rate of 150 cm^3 min^{-1} were used for catalytic tests. The catalytic tests were carried out at 170 and 220 °C. Catalyst bed temperature was measured and controlled using a J-type thermocouple and a PID controller-programmer. Before activity tests, the catalyst samples were reduced in H_2 flow (100 cm^3 min^{-1}) at 500 °C for 1 h. Gas stream at the reactor outlet was analyzed by on-line gas chromatography using a GC Varian CP 3380 equipped with flame ionization detector and a Graphpac GC 0.1% AT-1000 (80–100) packed column. It was verified that diffussional limitations do not alter the reaction rate measurements by carrying out experiments varying the particle size in the range 0.15–0.60 mm and the contact time between 10 and 80 g cat. h mol^{-1}.

3. Results and discussion

3.1. Catalyst characterization

The supports used in this work have different specific surface area (Sg), from 250 to 560 m^2 g^{-1}, and pore volume (Vp), from 0.24 to 0.88 cm^3 g^{-1} (Table 1). In addition, H-BEA is a molecular sieve with micropores of 0.67 nm in diameter, while SiO_2 and SiO_2–Al_2O_3 are mesoporous solids whose mean pore diameters (Dp) are 13.9 and 5.5 nm, respectively. The Sg, Vp and Dp values determined for Ni/SiO_2 and Ni/SiO_2–Al_2O_3 samples, after impregnation and calcination, are quite similar to those of the corresponding supports (Table 1). The lowest effect of nickel addition on textural properties was observed in the case of Ni/SiO_2. Instead, the greatest decrease in Sg and Vp after impregnation and calcination was observed for Ni/H-BEA. This would indicate that, during the impregnation and calcination sequence, some of the nickel precursor has blocked a fraction of the support micropores.

The chemical analysis by ICP was done in order to determine the real amount of nickel incorporated to each support. The results, shown in Table 2, are in good agreement with the theoretical values since, in all of the cases, the nickel load was between 9 and 10%, approximately.

The X-ray diffraction (XRD) patterns of the supports used in this work are shown in Fig. 2A. For SiO_2 and SiO_2–Al_2O_3, the characteristic silica amorphous halo, in the range 2θ = 15–30°, was only observed. On the other hand, the X-ray diffractogram for the H-BEA sample corresponds to the characteristic crystalline structure of zeolite Beta [16]. In summary, some of the supports used in this work are amorphous, as SiO_2 and SiO_2–Al_2O_3, or it has a very well-defined crystalline structure, as zeolite H-BEA.

The diffractograms of Ni oxides precursors supported on SiO_2, SiO_2–Al_2O_3 and zeolite H-BEA are shown in Fig. 2B. In all of the cases, new diffraction peaks at similar 2θ values were observed, which were assigned to a polycrystalline nickel oxide phase (JCPDS 22-1189). In all of the cases, the mean crystallite size, estimated by applying the Debye–Scherrer equation, was between 13 and 15 nm.

Table 1
Chemical composition, textural properties and concentration of surface acid sites of supports and precursors calcined in air flow at 500 °C.

Sample	Ratio Si/Al	Sg[a] ($m^2\ g^{-1}$)	Vp[b] ($cm^3\ g^{-1}$)	Dp[c] (nm)	TPD-NH_3 ($\mu mol\ m^{-2}$)
SiO_2	–	254	0.880	13.9	n.d.
SiO_2–Al_2O_3	6.62	467	0.676	5.54	1.09
H-BEA	12.5	560	0.240	0.67	0.90
Ni/SiO_2	–	250	0.851	14.5	n.d.
Ni/SiO_2–Al_2O_3	6.62	433	0.655	4.09	0.89
Ni/H-BEA	12.5	524	0.168	–	0.65

[a] *Sg*: specific surface.
[b] *Vp*: pore volume.
[c] *Dp*: pore diameter.

Table 2
Reduction degree (*RD*) and H_2 chemisorption capability of the nickel samples prepared in this work.

Catalyst	Ni[a] (%)	H_2^T[b] ($mmol\ g_{cat}^{-1}$)	H_2^E[c] ($mmol\ g_{cat}^{-1}$)	RD[d] (%)	H_2 $(HC)_i$[e] ($mmol\ H_2\ g_{cat}^{-1}$)
Ni/SiO_2	9.65	1.64	1.51	92	0.22
Ni/SiO_2–Al_2O_3	9.90	1.69	1.24	74	0.15
Ni/H-BEA	8.90	1.52	0.99	65	0.20

[a] Metal loading determined by ICP.
[b] Theoretical H_2 consumption calculated from NiO content.
[c] Experimental H_2 consumption calculated from TPR profiles.
[d] Reduction degree: $RD = (H_2^E/H_2^T) \times 100$.
[e] Hydrogen chemisorbed irreversibly after reduction in H_2 at 500 °C.

The TPR profiles of the nickel oxide precursors are presented in Fig. 3. In the case of Ni/SiO_2, only one reduction peak with a maximum H_2 uptake at 400 °C was detected, which is in agreement with that observed in previous works for the reduction of NiO supported on SiO_2 [15,17]. Besides, this peak is asymmetric and wide, which is indicative that large particles of NiO, with varying sizes, are involved in the reduction process. This is in good agreement with the XRD results obtained for Ni/SiO_2 oxide precursor. In the profile corresponding to Ni/SiO_2–Al_2O_3, two H_2 consumption peaks were observed. The first peak has a maximum at 380 °C, which can be again assigned to reduction of NiO particles. It is worth to notice that this H_2 consumption band started at 230 °C, i.e. 90 °C lower than in the case of Ni/SiO_2. This is indicating that some of the NiO particles on Ni/SiO_2–Al_2O_3 are smaller than those on Ni/SiO_2 and, in consequence, they are more easily reduced. The maximum of the second peak was observed at 520 °C and corresponds to the reduction of Ni^{2+} interacting strongly with the support, probably forming surface nickel aluminates [18,19]. Finally, the profile of Ni/H-BEA showed a H_2 consumption profile similar to that of Ni/SiO_2–Al_2O_3 with two peaks at 400 °C and 580 °C: the first peak was also assigned to the reduction of NiO particles of different sizes, while the second one was attributed to the reduction of Ni^{2+} strongly interacting with the support.

With the objective to get more information about Ni^{2+}–support interaction, the reduction degree (*RD*) for each sample was estimated as the ratio between the experimental H_2 consumption (H_2^E)

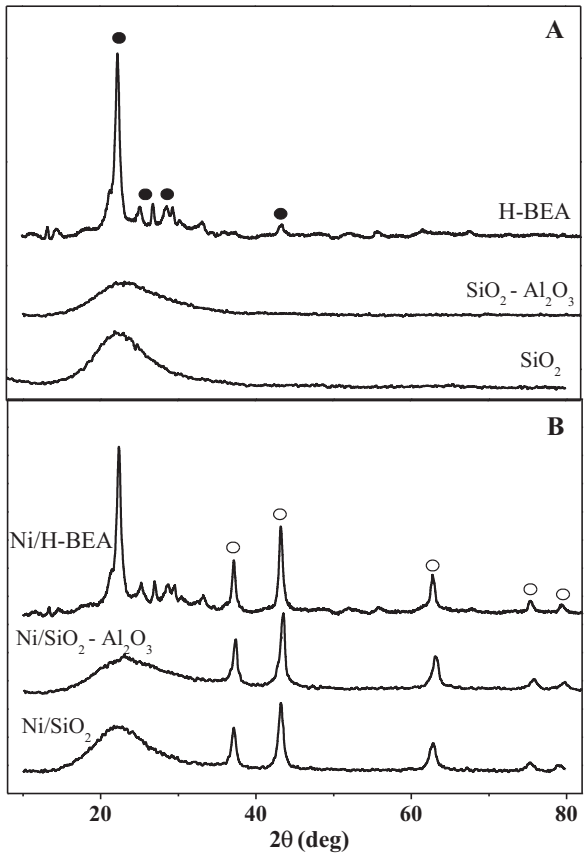

Fig. 2. XRD patterns for the supports (A) and nickel oxide precursors (B) after calcination at 500 °C. (●) H-BEA (JCPDS 48-0074); (○) NiO (JCPDS 22-1189).

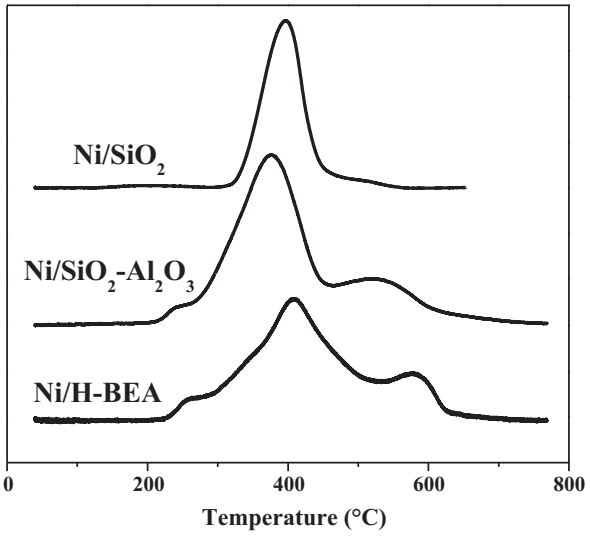

Fig. 3. TPR profiles of the nickel oxide precursors after calcination at 500 °C.

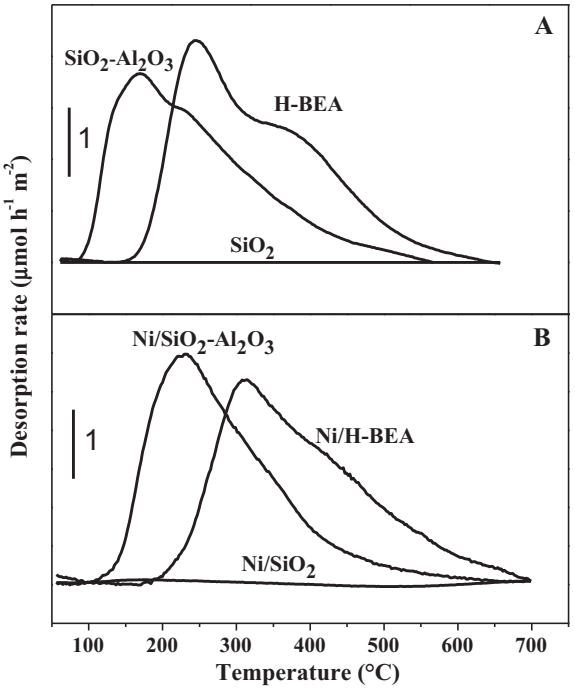

Fig. 4. TPD-NH_3 profiles (m/e = 16) for (A) supports and (B) nickel catalysts obtained after reduction in H_2 flow at 500 °C (NH_3 adsorption at 100 °C and desorption at 10 °C min^{-1}).

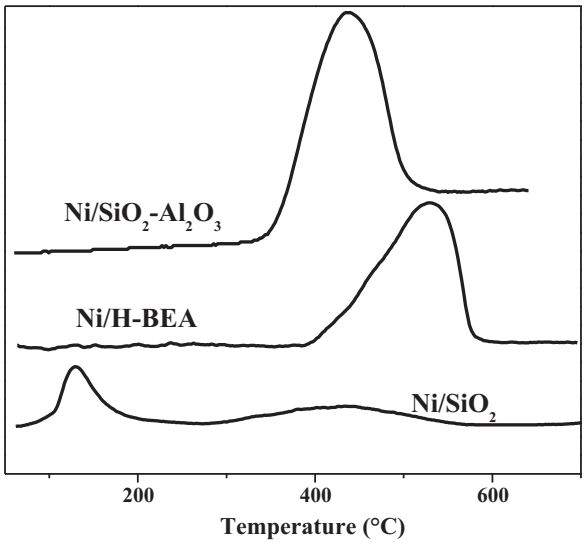

Fig. 5. H_2 signal (m/e = 2) in the TPD-NH_3 experiments with nickel catalysts obtained by reduction in H_2 flow at 500 °C (NH_3 adsorption at 100 °C and desorption at 10 °C min^{-1}).

and the theoretical H_2 consumption (H_2^T). The H_2^T values were calculated from the NiO content in each sample, determined from ICP analysis, and assuming a stoichiometry H_2:NiO = 1 [20]. The H_2^E values were estimated by numerical integration of the corresponding TPR profiles (Fig. 3). The obtained *RD* values are shown in Table 2. For all of the cases, it was verified that H_2^E was lower than H_2^T, indicating that part of de Ni^{2+} ions were not completely reduced during TPR experiments (Table 2). The higher *RD* value was observed for Ni/SiO_2, in which the interaction Ni^{2+}–support is low [21]. In this case, *RD* was 92%, very close to values previously reported for Ni/SiO_2 samples [22,23]. The *RD* value estimated for Ni/SiO_2–Al_2O_3 is usually explained by the formation of surface nickel silicates, ortho-silicates and/or aluminates, which could be reduced only at temperatures above 800 °C [18]. The high specific surface area of SiO_2–Al_2O_3 could promote the formation of these kinds of compounds. The lowest *RD* value was determined for Ni/H-BEA, in agreement with the fact that the reducibility of Ni^{2+} ions interacting very strongly with aluminosilicate surfaces is very low [24]. In the case of Ni/H-BEA, some H^+ exchange by Ni^{2+} can occur. These exchanged Ni^{2+} ions are stabilized in the surface sites inside the zeolite microporous and, as a consequence, their reducibility is very low [25]. It is also possible that the smallest NiO particles, formed during the calcination, have reacted with H^+ on the zeolite surface to give $Ni(OH)^+$. These $Ni(OH)^+$ ions can also interact strongly with the zeolite surface and, as a consequence, these $Ni(OH)^+$ surface species have a very low reducibility [25]. In summary, TPR profiles and *RD* values are indicating that Ni^{2+}–support interaction follows the pattern: Ni/SiO_2 < Ni/SiO_2–Al_2O_3 < Ni/H-BEA.

In all of the cases, the amount of irreversibly chemisorbed H_2 was similar indicating that the dispersion of metal nickel is low and almost the same on the different supports used in this work (Table 2). These results are in agreement with those obtained by XRD, which showed that, in all of the cases, rather large NiO crystallites are formed after calcination. Thus, it is expected that a poorly dispersed metal nickel phase will be obtained from these oxide precursors.

The evolutions of NH_3 desorption (m/e = 16) from supports are shown in Fig. 4A. It was observed that the desorption of NH_3 from SiO_2–Al_2O_3 starts at 100 °C and continues until 570 °C, reaching a maximum at 160 °C. For H-BEA, the desorption begun at 150 °C and finished approximately at 650 °C, reaching a maximum at 230 °C. These temperature ranges are indicating that both SiO_2–Al_2O_3 and H-BEA have surface sites with a wide range of acid strength. In addition, both mixed oxides showed similar amounts of NH_3 adsorbed per surface unit (Table 1). Instead, no NH_3 desorption was detected in the case of SiO_2, indicating that there are not acid sites on its surface with the capability to interact with NH_3 (Fig. 4A and Table 1).

During TPD-NH_3 experiments of Ni-supported samples, previously reduced at 500 °C in H_2 flow, the evolutions of m/e = 2 (Fig. 5) and 28 (not shown) signals were observed besides the one of m/e = 16 signal (Fig. 4B). It must be noted that NH_3 desorption from Ni/SiO_2–Al_2O_3 and Ni/H-BEA occurred in the same temperature range than for the corresponding supports, i.e. SiO_2–Al_2O_3 and H-BEA (Fig. 4A and B). However, after impregnation with Ni, a decrease in the total amount of desorbed NH_3 was observed (Fig. 4 and Table 1). The deconvolution of all of the NH_3 TPD profiles was satisfactorily carried out considering three Gaussian peaks (Table 3). This result is interpreted as if three types of sites with different acid strength are present on the surface of supports used in this work. Then, it was concluded that the diminution in the total amount of desorbed NH_3 was mainly due to that one desorbed at T > 300 °C. This was probably due to selective blocking of the strongest acid sites by the nickel deposited on both H-BEA and SiO_2–Al_2O_3 surfaces. Thus, it is likely that the high Ni^{2+}–support interaction observed with SiO_2–Al_2O_3 and H-BEA is due to selective adsorption of Ni^{2+} on the strongest acid sites, i.e. surface acid sites that desorbs NH_3 at T > 300 °C. This type of interaction is not possible with SiO_2 since this oxide lacks of strong acid sites. On the other hand, the evolutions with temperature for m/e = 2 and 28 shows that some NH_3 was adsorbed on the metal nickel surface and it desorbs dissociatively giving H_2 and N_2 as the temperature was raised during TPD experiment. The evolution corresponding to m/e = 2 is shown in Fig. 5. A similar evolution was observed for m/e = 28 in the same temperature intervals (not shown), in agreement with the fact that both H_2 and N_2 are coming from the decomposition of NH_3 adsorbed on metal nickel surface. From these TPD profiles, it was concluded that Ni/SiO_2–Al_2O_3 and Ni/H-BEA are more active for the adsorption and dissociative desorption of NH_3 than Ni/SiO_2.

Table 3
Gaussian deconvolution of TPD-NH_3 signals (m/e = 16) obtained with supports and nickel based catalysts.

Sample	Peak 1		Peak 2		Peak 3	
	A_1 [a] (a.u.)	T_1 [b] (°C)	A_2 [a] (a.u.)	T_2 [b] (°C)	A_3 [a] (a.u.)	T_3 [b] (°C)
SiO_2–Al_2O_3	155	143	254	203	285	295
Ni/SiO_2–Al_2O_3	200	211	264	289	104	411
H-BEA	163	219	139	257	470	345
Ni/H-BEA	167	300	215	377	177	482

[a] Areas under each curve determined by Gaussian deconvolution.
[b] Temperatures at the maximum of each deconvolution peak.

It is well accepted that NH_3 decomposition on metal catalysts is a structure sensitive reaction [26,27]. Then, it is assumed that the metal surface on Ni/SiO_2 is different than that one obtained on Ni/SiO_2–Al_2O_3 and Ni/H-BEA. The last is in agreement with TPR profiles showing that not only large NiO particles but also small NiO particles on SiO_2–Al_2O_3 and Ni^{2+} interacting strongly with SiO_2–Al_2O_3 and H-BEA surface are present. Thus, the reduction in H_2 flow at 500 °C will lead to different metal nickel surfaces depending on the Ni^{2+}–support interaction. More specifically, it is expected that reduction of these nickel species, present on SiO_2–Al_2O_3 and H-BEA surface, will lead to the formation of small metal nickel particles, in addition to the large ones formed from large NiO particles. This explanation is in agreement with the results obtained in the NH_3 decomposition, which is a structure sensitive reaction.

In summary, after impregnation and the subsequent calcination, a set of nickel oxide precursors containing similar metal loads, close to 10%, was obtained. The *Vp* and *Sg* of SiO_2 and SiO_2–Al_2O_3 were maintained approximately constant indicating that the textural properties are not substantially affected after impregnation and calcination. Instead, the *Vp* in H-BEA diminished substantially after impregnation and calcination, probably due to partial blockage of micropores. XRD results confirmed the formation of a polycrystalline NiO phase on all of the supports. However, TPR and TPD-NH_3 experiments confirm that an important fraction of Ni^{2+} ions are strongly interacting with the surface of SiO_2–Al_2O_3 and H-BEA and also small NiO particles are formed on SiO_2–Al_2O_3 surface. As a consequence, an active metal nickel surface for adsorption and dissociative desorption of NH_3 is formed over both supports, after reduction in H_2 flow at 500 °C. Instead, the Ni^{2+}–SiO_2 interaction is very low and the metal nickel phase formed in this case has a poor activity for the adsorption and dissociative desorption of NH_3. Thus, these physicochemical characterization results are clearly indicating that the metal nickel surfaces formed on the three supports are structurally different.

3.2. Catalytic tests

Catalytic tests were carried out at 170 °C and 220 °C, with a $W/F^0_{MA} = 12\,g\ h\ mol^{-1}$ and under atmospheric pressure. In first place, blank experiments using the three supports were carried out and none activity was observed. Then, any intrinsic activity of the support in the gas phase MA hydrogenation was discarded for the conditions used in this work. With Ni-supported catalysts, in all of the cases, the only products detected and analyzed were SA, GBL, PA and CH_4. All of Ni catalysts were very active for gas phase MA hydrogenation and the MA conversions were always close to 100%, remaining constant during the whole catalytic test. Thus, MA molecule is adsorbed on the available Ni metallic sites and reacts very fast with the H_2 chemisorbed on the metal surface to give SA selectively. In a previous work, using a Ni//SiO_2 catalyst, we showed that GBL and PA are mainly coming from SA hydrogenolysis [15], as it is shown in Fig. 1. Then, it is possible to analyze the evolutions of GBL and PA productions at different levels of SA conversion.

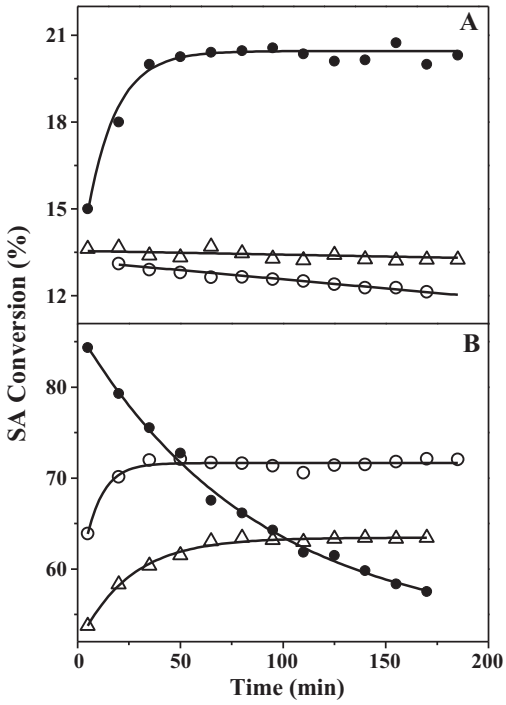

Fig. 6. Succinic anhydride (SA) conversion as a function of time at (A) 170 °C and (B) 220 °C (P = 1 bar; $W/F^0_{MA} = 11.9\,g\ h\ mol^{-1}$). (○) Ni/$SiO_2$, (△) Ni/$SiO_2$–$Al_2O_3$, (●) Ni/H-BEA.

The evolutions of SA conversion with time at 170 °C are shown in Fig. 6A for the three Ni-based catalysts. With Ni/SiO_2 and Ni/SiO_2–Al_2O_3 catalysts, the initial SA conversion was approximately 13–14% (Table 4) and then remained almost constant during the 3 hours of catalytic test. With Ni/H-BEA catalyst, the initial SA conversion was 15% but then increased to 20% in 45 minutes of reaction. This type of evolution was previously explained by assuming that SA, formed from MA hydrogenation, desorbs from hydrogenating nickel sites faster than SA adsorbs on hydrogenolytic nickel sites to be converted into GBL and PA [15]. Thus, the amount of SA desorbed from hydrogenation sites and SA conversion increase

Table 4
Succinic anhydride (SA) conversion and selectivity to γ-butyrolactone (GBL) with Ni-based catalysts (P = 1 bar; $W/F^0_{MA} = 12\,g\ h\ mol^{-1}$).

Sample	T (°C)	X^0_{SA} [a] (%)	S^0_{GBL} [a] (%)	X_{SA} [b] (%)	S_{GBL} [b] (%)
Ni/SiO_2	170	12.9	55.0	12.3	44.0
	220	63.8	58.8	72.0	52.2
Ni/SiO_2–Al_2O_3	170	13.9	85.9	13.9	84.1
	220	53.9	87.6	63.4	87.7
Ni/H-BEA	170	15.0	68.0	19.9	74.2
	220	84.5	87.7	57.6	79.3

[a] Initial SA conversion (X^0_{SA}) and selectivity to GBL [$S^0_{GBL} = Y^0_{GBL}/(Y^0_{GBL} + Y^0_{PA})$].
[b] SA conversion (X_{SA}) and selectivity to GBL [$S_{GBL} = Y_{GBL}/(Y_{GBL} + Y_{PA})$] after 3 hours of reaction.

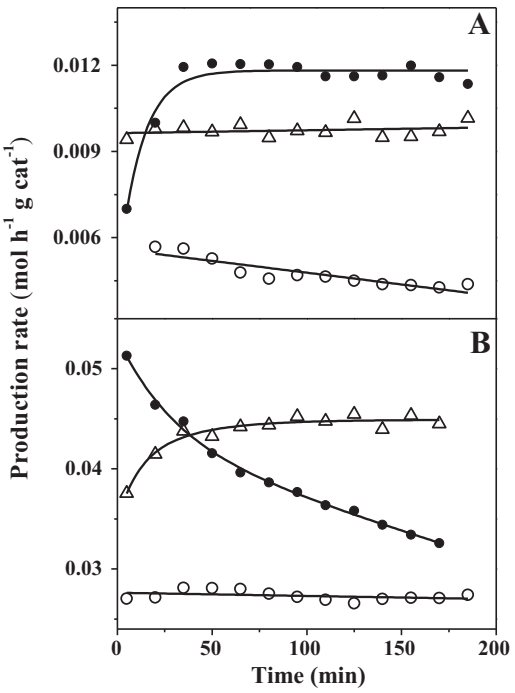

Fig. 7. Production rates of GBL as a function of time at (A) 170 °C and (B) 220 °C (P = 1 bar; W/F^0_{MA} = 11.9 g h mol^{-1}). (○) Ni/SiO_2, (△) Ni/SiO_2–Al_2O_3, (●) Ni/H-BEA.

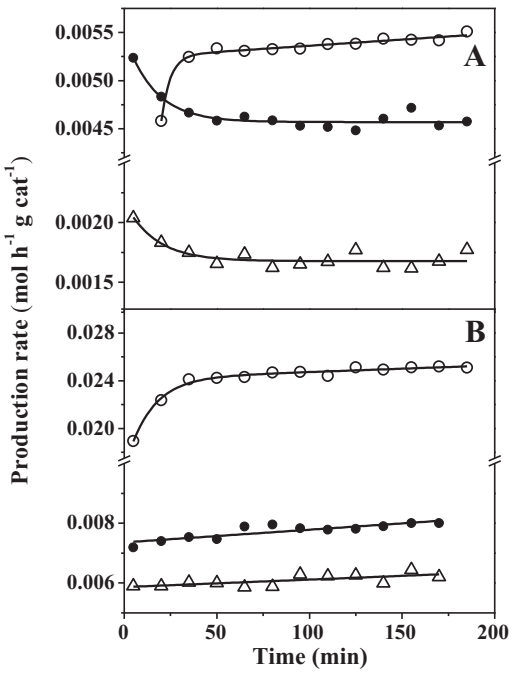

Fig. 8. Production rates of PA as a function of time at (A) 170 °C and (B) 220 °C (P = 1 bar; W/F^0_{MA} = 11.9 g h mol^{-1}). (○) Ni/SiO_2, (△) Ni/SiO_2–Al_2O_3, (●) Ni/H-BEA.

until a steady state is reached for the surface concentration of SA adsorbed on hydrogenolytic sites and the amount desorbed from hydrogenation sites.

At 220 °C, Ni/SiO_2–Al_2O_3 and Ni/SiO_2 catalysts gave evolutions with increasing SA conversion with time (Fig. 6B), similar to that observed with Ni/H-BEA at 170 °C. This is indicating that, at 220 °C, SA adsorption becomes the limiting step for SA hydrogenolysis on Ni/SiO_2–Al_2O_3 and Ni/SiO_2. The initial SA conversion with Ni/SiO_2 was almost 64% and then rapidly increased to 72%. With Ni/SiO_2–Al_2O_3, the initial SA conversion was approximately 54% and then slowly increased to 63%. Ni/H-BEA showed again a completely different behavior to that of the mesoporous solids: the initial SA conversion was about 85% and then decreased monotonically during the catalytic test up to 58%, without reaching the steady state. It is very likely that some compounds, formed during the hydrogenation–hydrogenolysis sequence, remain strongly adsorbed on Ni/H-BEA blocking the micropores. However, it is worth noting that a selective deactivation of the hydrogenolytic sites took place, since GBL formation rate diminished with time while PA formation rate kept almost constant (Figs. 7B and 8B). A plausible explanation could be that the pore blockage is progressively reducing the accessibility of SA to the small metal particles located in the micropores, which would be selective for SA hydrogenolysis into GBL. Large metal particles placed on the external surface of H-BEA, which would be selective for SA hydrogenolysis into PA, are not affected by this deactivation. In summary, at 220 °C, Ni/H-BEA was initially the most active in the SA hydrogenolysis, but suffered an important deactivation during reaction. The above results are showing that the initial SA conversion and its evolution with time on stream depend strongly on the nature of Ni–support system and reaction temperature.

The evolutions for the production rates of GBL and PA with time on stream are shown in Figs. 7 and 8. These evolutions are reinforcing the ratio between catalytic performance and the differences already observed for the three samples in the physicochemical characterization. At 170 °C, the initial yield in CH_4 was always lower than 0.5% with the three catalysts. This is indicative that initially the main reaction pathway is the hydrogenolysis of SA into GBL and PA, while GBL hydrogenolysis into PA is not significant (Fig. 1). When Ni/SiO_2 was used as catalyst, a slight diminution of the GBL production rate with time on stream was observed, while PA production rate increased in similar grade (Figs. 7A and 8A). The decrease in selectivity to GBL, from 55 to 44% (Table 4), may be explained from these evolutions with time. These results are indicating that a small amount of GBL is slowly converted into PA during the run. For Ni/SiO_2–Al_2O_3, the GBL production rate remains practically constant during the 3 hours of catalytic test (Fig. 7A), while PA production rate diminished slightly (Fig. 8A). As a consequence, the selectivity to GBL remains almost constant at 85% (Table 4). In the case of Ni/H-BEA, GBL production rate increase and PA production rate diminished until a steady state was reached (Figs. 7A and 8A), being the increase in GBL production more important than the diminution in PA one. These two evolutions are indicating that: (1) there is a slow SA adsorption on the hydrogenolytic sites that give GBL, as it was discussed above; (2) a selective deactivation of sites that are active for SA hydrogenolysis into PA is occurring. As a consequence, the selectivity to GBL increased from 68 to 74% during the run at 170 °C (Table 4).

At 220 °C, the yield in CH_4 was higher than at 170 °C, indicating that GBL hydrogenolysis into PA became more important (Fig. 1). The yields in CH_4 were 5% with Ni/SiO_2, 2% with Ni/SiO_2–Al_2O_3 and 9% with Ni/H-BEA. Thus, even at 220 °C, the hydrogenolysis of GBL into PA is still less important than the previous hydrogenolysis of SA into GBL and PA, especially in the case of Ni/SiO_2–Al_2O_3. The trends observed for GBL and PA production at 220 °C (Figs. 7B and 8B) were different to those observed at 170 °C (Figs. 7A and 8A). With Ni/SiO_2, PA and GBL production rates are comparable. GBL production rate kept constant during the 3 hours of reaction, while a small increase in PA production rate was observed with an evolution similar to the one observed for X_{SA} with time on stream (Fig. 6B). Thus, selectivity to GBL diminished from 59 to 52% during the run (Table 4), similar to what happened at 170 °C. The trends with Ni/SiO_2–Al_2O_3 were opposite to those observed with Ni/SiO_2: while GBL production rate increased, until a steady state was reached, the PA production rate kept constant with time on stream (Figs. 7B and 8B).

In this case, not only the yield in CH_4 was the lowest, but GBL production was much more important than PA one. This means that the main reaction pathway with $Ni/SiO_2–Al_2O_3$ was the selective hydrogenolysis of SA into GBL. Thus, selectivity to GBL was about 88% (Table 4) and it kept almost constant during the whole run. Finally, the trends with Ni/H-BEA showed a very important decay for GBL production rate with time on stream, while amazingly PA production rate kept almost constant (Figs. 7B and 8B). This is almost the opposite behavior to that observed at 170 °C with the same catalyst (Figs. 7A and 8A). Thus, with Ni/H-BEA, the selectivity to GBL diminished from 88 to 79% (Table 4) during the 3 hour run. These results are indicating that the active sites for SA hydrogenolysis on Ni/H-BEA are suffering an important selective deactivation during the reaction, i.e. especially the sites that are active for SA hydrogenolysis into GBL. Then, this selective deactivation becomes more important with temperature, which is opposite to that observed for Ni/SiO_2 catalyst.

From the results obtained at 220 °C, the following initial activity pattern is suggested: Ni/H-BEA > Ni/SiO_2 > $Ni/SiO_2–Al_2O_3$. However, after 3 hours, this pattern changed to: Ni/SiO_2 > $Ni/SiO_2–Al_2O_3$ > Ni/H-BEA. These results indicate that $Ni/SiO_2–Al_2O_3$ and Ni/SiO_2 catalysts were more stable than Ni/H-BEA, especially at the highest temperature used in this work. The activity loss of Ni/H-BEA is mainly due to deactivation of hydrogenolytic sites, probably due to micropore blockage by compounds formed during reaction. The pattern for initial selectivity to GBL at 220 °C can be resumed as follows: Ni/H-BEA ≅ $Ni/SiO_2–Al_2O_3$ > Ni/SiO_2. However, after 3 hours on stream at 220 °C, the pattern changed to: $Ni/SiO_2–Al_2O_3$ > Ni/H-BEA > Ni/SiO_2. This is because the deactivation of Ni/H-BEA is affecting selectively the conversion of SA into GBL during the catalytic test. Ni/SiO_2 was more active than $Ni/SiO_2–Al_2O_3$. However, the large metal particle formed on Ni/SiO_2 is favoring the formation of a metal nickel surface with sites that promote planar adsorption of SA and the subsequent preferential hydrogenolysis into PA. Instead, small metal nickel particles formed on $Ni/SiO_2–Al_2O_3$, from reduction of small NiO particles and Ni^{2+} interacting strongly with support surface, would be more selective for SA hydrogenolysis into GBL.

In summary, selective hydrogenolysis of SA into GBL with Ni-based catalysts is strongly depending on the nature of support and reaction conditions. The highest stability, production rate and selectivity to GBL were obtained at 220 °C with $Ni/SiO_2–Al_2O_3$. This catalyst has an intermediate interaction Ni^{2+}–support for the series used in this work, indicating that there is an optimum interaction that favors the formation of a metallic nickel surface that is active, stable and selective for the hydrogenolysis of SA into GBL. If the interaction Ni^{2+}–support is very low, as in the case of Ni/SiO_2, an active and stable metal nickel phase is formed, but with lower selectivity to GBL. Finally, if the Ni^{2+}–support interaction is too high, a very active and selective metal nickel phase is obtained, but with poor stability, especially at high temperature.

4. Conclusions

It was shown that the support nature affects the activity, selectivity and stability of Ni-based catalysts in the gas phase hydrogenation of maleic anhydride. This effect is clearly influencing the step of hydrogenolysis of succinic anhydride over nickel, in which γ-butyrolactone and propionic acid are obtained as main products. The Ni^{2+}–support interaction in the oxide precursor has an important influence over the final structure of the metallic nickel surface, as it was showed by temperature programmed decomposition of NH_3, a structure sensitive reaction. The Ni^{2+}–support interaction can be regulated by the concentration and strength of the acid sites on the support surface. Thus, the pattern found for Ni^{2+}–support interaction is: Ni/H-BEA > $Ni/SiO_2–Al_2O_3$ > Ni/SiO_2. The surface structure of the active metal nickel phase is strongly depending on this interaction degree. In this work, it was shown that the surface structure of metal nickel and, as a consequence, the performance of Ni-based catalyst on the selective hydrogenolysis of succinic anhydride into γ-butyrolactone, that is also a structure sensitive reaction, can be optimized by modulating the Ni^{2+}–support interaction. The best stability and GBL production is reached when a medium Ni^{2+}–support interaction is obtained, as in the case of $Ni/SiO_2–Al_2O_3$ catalyst. Thus, a selectivity as high as 88%, at succinic anhydride conversions of 60% or higher, are obtained at 220 °C. If the Ni^{2+}–support interaction is too low, as in the case of Ni/SiO_2, the metal nickel surface is more selective for the hydrogenolysis of succinic anhydride into propionic acid than in the case of $Ni/SiO_2–Al_2O_3$. If the interaction is too high, as in the case of Ni/H-BEA, a loss of stability is observed during the run due to selective blockage of hydrogenolytic sites located in the micropores of the zeolite, probably by strong adsorption of carbon compounds formed during reaction, especially at 220 °C.

References

[1] M. Messori, A. Vaccari, J. Catal. 150 (1994) 177–185.
[2] R. Zhang, H. Yin, D. Zhang, L. Qi, H. Lu, Y. Shen, T. Jiang, Chem. Eng. J. 140 (2008) 488–496.
[3] G. Budroni, A. Corma, J. Catal. 257 (2008) 403–408.
[4] G.L. Castiglioni, A. Vaccari, G. Fierro, M. Inversi, M. Lo Jacono, G. Minelli, I. Pettiti, P. Porta, M. Gazzano, Appl. Catal. A: Gen. 123 (1995) 132–144.
[5] Y.L. Zhu, J. Yang, G.Q. Dong, H.Y. Zheng, H.H. Zhang, H.W. Xiang, Y.W. Li, Appl. Catal. B: Environ. 57 (2005) 183–190.
[6] H. Jeong, T.H. Kim, K.I. Kim, S.H. Cho, Fuel Process. Technol. 87 (2006) 497–503.
[7] S.H. Vaidya, C.V. Rode, R.V. Chaudhari, Catal. Commun. 8 (2007) 340–344.
[8] S.M. Jung, E. Godard, S.Y. Jung, K.C. Park, J.U. Choi, J. Mol. Catal. A: Chem. 198 (2003) 297–302.
[9] W. Lu, G. Lu, Y. Guo, Y. Guo, Y. Wang, Catal. Commun. 4 (2003) 177–181.
[10] C. Ohlinger, B. Kraushaar-Czarnetzki, Chem. Eng. Sci. 58 (2003) 1453–1461.
[11] A.J. Marchi, J.L.G. Fierro, J. Santamaría, A. Monzon, Appl. Catal. A: Gen. 142 (1996) 375–386.
[12] C.I. Meyer, A.J. Marchi, A. Monzón, T.F. Garetto, Appl. Catal. A: Gen. 367 (2009) 122–129.
[13] S. Qi, B.A. Cheney, R. Zheng, W.W. Lonergan, W. Yu, J.G. Chen, Appl. Catal. A: Gen. 393 (2011) 44–49.
[14] A. Saadi, R. Merabti, Z. Rassoult, M.M. Bettahar, J. Mol. Catal. A: Chem. 253 (2006) 79–85.
[15] C.I. Meyer, S.A. Regenhardt, A.J. Marchi, T.F. Garetto, Appl. Catal. A: Gen. 417–418 (2012) 59–65.
[16] A. Simon-Masseron, J.P. Marques, J.M. Lopes, F. Ramoa Ribeiro, I. Gener, M. Guisnet, Appl. Catal. A: Gen. 316 (2007) 75–82.
[17] R. Fréty, L. Tournayan, M. Primet, G. Bergeret, M. Guenin, J.B. Baumgartner, A. Borgna, J. Chem. Soc. Faraday Trans. 89 (17) (1993) 3313–3318.
[18] P. Castaño, B. Pawelec, J.L.G. Fierro, J.M. Arandes, J. Bilbao, Fuel 86 (2007) 2262–2274.
[19] S.R. Kirumakki, B.G. Shpeizer, G.V. Sagar, K. Chary, A. Clearfield, J. Catal. 242 (2006) 319–331.
[20] E.G.M. Kuijpers, M.W.C.M.A. Nieuwesteeg, G.J. Wermer, J.W. Geus, J. Catal. 112 (1988) 107–115.
[21] N.M. Bertero, A.F. Trasarti, C.R. Apesteguía, A.J. Marchi, Appl. Catal. A: Gen. 394 (2011) 228–238.
[22] H. van't Blik, R. Prins, J. Catal. 97 (1986) 188–199.
[23] E. van Steen, G.S. Sewell, R.A. Makhote, C. Micklethwaite, H. Manstein, M. de Lange, C.T. O'Connor, J. Catal. 162 (1996) 220–229.
[24] C.M.N. Yoshioka, M.H. Jordao, D. Zanchet, T.F. Garetto, D. Cardoso, Appl. Catal. A: Gen. 355 (2009) 20–26.
[25] A. Fúnez, A. de Lucas, P. Sánchez, M.J. Ramos, J.L. Valverde, Chem. Eng. J. 136 (2008) 267–275.
[26] C. Plana, S. Amenise, A. Monzón, E. García-Bordejé, J. Catal. 275 (2010) 228–235.
[27] X.-K. Li, W.-J. Ji, J. Zhao, S.-J. Wang, C.-T. Au, J. Catal. 236 (2005) 181–189.